IOP Publishing Plasma Sources Science and Technology

Plasma Sources Sci. Technol. **23** (2014) 015006 (13pp) doi:10.1088/0963-0252/23/1/015006

Analysis of resonant planar dissipative network antennas for rf inductively coupled plasma sources

Ph Guittienne[1], A A Howling[2] and Ch Hollenstein[2]

[1] Helyssen, Route de la Louche 31, CH-1092 Belmont-sur-Lausanne, Switzerland
[2] Ecole Polytechnique Fédérale de Lausanne (EPFL), Centre de Recherches en Physique des Plasmas, CH-1015 Lausanne, Switzerland

Received 1 July 2013, revised 5 November 2013
Accepted for publication 25 November 2013
Published 10 January 2014

Abstract

The analysis of a radio-frequency (RF) planar antenna is presented for applications in plasma processing. The antenna is a network of elementary meshes composed of inductive and capacitive elements which exhibits a set of resonant modes. The high currents generated by RF power feeding under resonance are efficient for plasma generation. A general solution is derived for the currents in the driven dissipative network for these conditions. The dominantly real input impedance near antenna resonance avoids the high reactive currents and voltages in the matching box and RF power connections which can be a problem with conventional large-area capacitively and inductively coupled plasma sources. The driven antenna can be approximated by a parallel resonance equivalent circuit whose input impedance can conveniently be measured to interpret the dissipation due to the plasma.

1. Introduction

Plasmas are used for various applications such as solar cell production, semiconductor manufacturing, food packaging and space propulsion, to name just a few. There is a constant need to improve plasma sources in order to increase the process rates and to develop new types of products. One aspect of source performance is the requirement of high electron density, since a dense plasma generally leads to high dissociation rates and an efficient use of the process precursors. A second important aspect lies in the possibility of large-area plasma processing. This has a double interest as it would allow larger amounts of small pieces to be treated in a single run as well as larger work-pieces to be processed.

Radio-frequency (RF) driven discharges are commonly used for high density plasma sources [1]. Considerable difficulties are often met in the generation of very large-area plasma with regard to the RF power injection, because conventional RF sources present almost purely reactive input impedance which tends either towards zero (capacitive discharges) or towards infinity (inductive discharges) with increasing area. The impedance matching between the RF generator and the source then drives very high currents and/or voltages in the matching network and power feed lines.

These limitations could be overcome using RF network antennas (Helyssen sources) whose essential characteristic is that they are resonant devices. When excited at one of its resonance frequencies the antenna develops very high currents within its structure, which can be used for inductively coupled plasma sources [2–4]. These resonating current distributions are called the normal modes of the antenna and are characterized by their sinusoidal distribution [5]. In addition to the fact that the high current distributions generated at resonance are very efficient in terms of plasma generation, a major advantage of these antennas lies in their input impedance properties which could allow very large-area plasma sources to be developed. In its cylindrical version (closed configuration), the Helyssen antenna was shown to be well-adapted for plasma generation by helicon wave excitation in the presence of a static magnetic field [6].

A planar version of a resonant antenna was recently constructed and showed good performance in terms of plasma uniformity and high electron density [2–4]. Measurements of the antenna impedance [2] showed that it behaved as a parallel resonance circuit in the neighborhood of a resonant mode. A dissipative network model is developed here to interpret those measurements in terms of the effect of plasma coupling on the antenna component values. This model also provides a

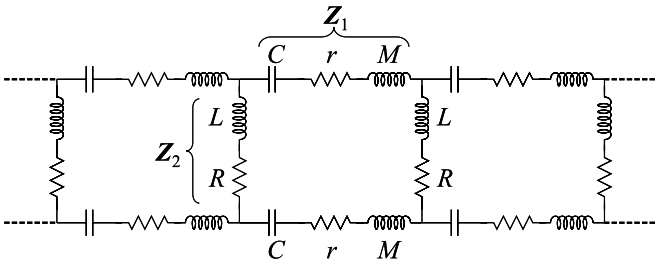

Figure 1. High-pass dissipative ladder network made up of identical meshes, showing the leg inductances L with resistances R, linked by capacitances C with short connections of inductance M and resistance r.

basic theoretical framework to optimize the antenna design with regard to current uniformity and input impedance, in order to further develop the resonant network for plasma source applications. Experimental measurements of the influence of the mode structure on plasma uniformity [7] will be discussed in future work.

The first part of this study describes the normal modes of the antenna, the second part gives a general solution for the currents of driven dissipative antennas, and in the third part, a parallel resonance equivalent circuit is derived in terms of the antenna components and their modifications due to plasma coupling.

2. Resonant planar network as an inductively coupled plasma source

This work describes the principles of the Helyssen planar antenna [8]. Its structure and operating principles are similar to the closed cylindrical birdcage antenna previously described [5, 6], but it is unwrapped to form an open and planar structure, as shown in figure 1. The planar structure is a segment of a ladder network which can also be called an open coil (or antenna) in the literature [5]. The planar antenna is suited for surface treatment of large flat areas, whereas the cylindrical version can be used as a volume plasma source for immersion of work-pieces [7]. Even though their applications are different, the circuit analysis of open and closed antennas is only distinguished by the boundary conditions inherent to their structure [5]. The closed antenna (birdcage) is well known for nuclear magnetic resonance (NMR) measurements where the $m = 1$ mode is used to generate a uniform RF magnetic field to excite the nuclear spins in biological samples [5]. Driven birdcage resonators with losses were recently considered by Novikov [9] using low impedance voltage sources applied to single mesh elements. Pascone *et al* [10] and Tropp [11] treated the birdcage resonator as a lossy transmission line. Other authors [12, 13] represented the dissipation as an effective coil resistance. In this paper, we consider the general case of a dissipative planar resonant antenna, with arbitrary positions for the RF connections along one side, applied as a plasma source.

Throughout this work, a discrete component (lumped element) equivalent circuit analysis will be used. This is valid provided that all circuit dimensions are small compared with the wavelength of the RF excitation. Electromagnetic effects due to large dimensions and high frequencies will be considered in later work.

The balanced high-pass passive filter ladder network shown in figure 1 has shunt inductors and series capacitors. The inductors consist of conducting legs (rungs), regularly distributed, with each one connected at both ends to its closest neighbors by capacitors. In the RF range (1–100 MHz), the legs can be approximated by self-inductances L having a small resistance R. The high-quality-factor capacitors C in the two side-branches (the stringers) have metal leads to link the rungs together, having self-inductance M and resistance r. To a first order approximation for a dissipative antenna, therefore, the stringer impedances are $Z_1 = 1/(\mathrm{j}\omega C) + \mathrm{j}\omega M + r$, and the leg impedances are $Z_2 = R + \mathrm{j}\omega L$, where ω is the RF angular frequency. The mutual inductance between all conducting parts has a strong influence on the mode frequencies [5], but its calculation is beyond the scope of this work. On the other hand, the mode structure of the currents and voltages calculated here is not strongly perturbed by the mutual inductance effect [2]. The general formulation given in this work can be applied to any configuration provided that the network is made up of identical elementary meshes. We consider high-pass networks as a specific example for plasma applications, although other resonant antenna configurations can also be envisaged (low-pass, hybrid, etc).

Experiments on rf network antennas for large-area and large-volume inductively coupled plasma sources have been described in [7] where it was shown that further understanding of the antenna–plasma coupling requires an analysis of the dissipative network antenna. As an example, the data points in figure 2(*a*) show the impedance of a planar 23-leg antenna measured without plasma [2]. The fitted line demonstrates that the network of figure 1 can be well represented by a parallel resonance equivalent circuit. In the presence of a low pressure gas, capacitive coupling from the high-voltage points on the antenna ignites a plasma; the antenna input impedance does not change significantly because the capacitance between the antenna and plasma is small compared with the antenna capacitances C [7]. As the antenna input power is raised, currents induced in the plasma then cause a transition to an inductively coupled plasma [7, 14–18]. The input impedance of the antenna changes strongly as shown by the example in figure 2(*b*). This change is due to plasma–antenna coupling by transformer action as described by Piejak *et al* [14].

In this case, each leg in figure 1 can be considered to be a primary circuit (self-inductance L_0, resistance R_0, in figure 3) which induces a skin current in the plasma. This induced current can be considered as a secondary circuit having a geometric (or magnetic) self-inductance L_2 and a plasma impedance [14]. The plasma impedance is proportional to the plasma complex (vector) resistivity $\rho = (\nu + \mathrm{j}\omega)m_\mathrm{e}/(n_\mathrm{e}e^2)$, where m_e and n_e are the electron mass and number density and ν is the effective electron collision frequency due to collisions with the neutral gas [1]. Hence, if the resistance of the plasma current path in the secondary circuit has a value R_2, then the reactance of this plasma current path is $\mathrm{j}\omega R_2/\nu$, with respect to the ratio of the real and imaginary parts of the plasma resistivity. This plasma reactance can be written as an effective plasma

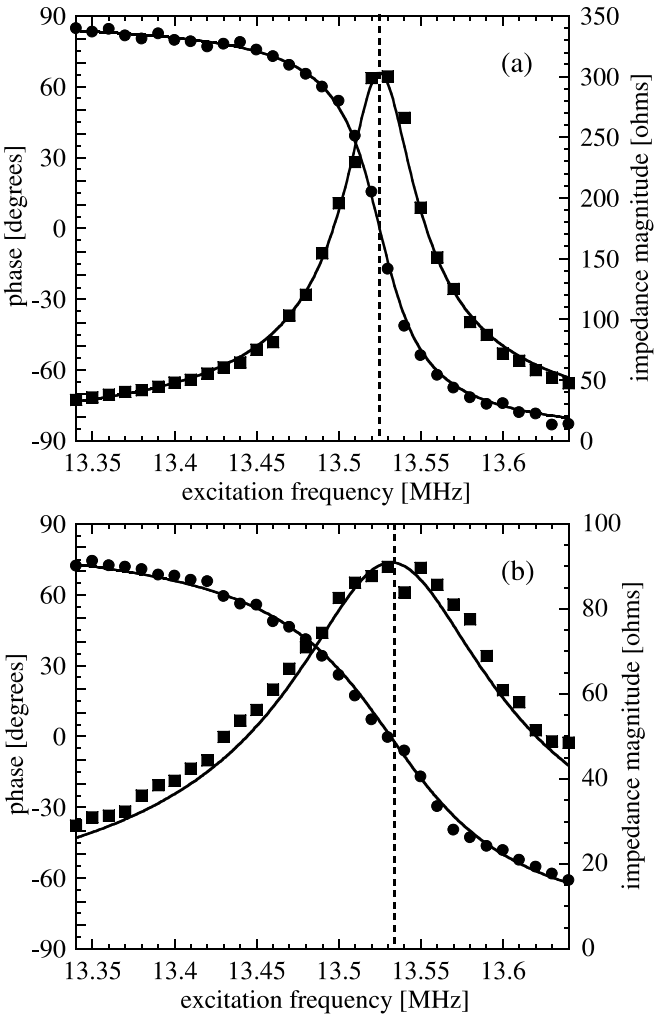

Figure 2. The antenna impedance magnitude (squares) and phase (circles) measured in the neighborhood of the $m = 6$ mode (a) without plasma; and (b) with a low power plasma (80 W) in 5 Pa of argon. The lines show fitted curves using a parallel resonance equivalent circuit for each case: (a) 13.13 nF in parallel with a series combination of 10.55 nH and 2.65 mΩ; (b) 15.09 nF in parallel with a series combination of 9.166 nH and 6.68 mΩ. The dotted lines show the shift in the resonance frequency from 13.525 MHz (without plasma) to 13.532 MHz for the low power plasma. Data taken from [2].

inductance $L_e = R_2/\nu$, as shown schematically in figure 3, which is physically due to electron inertia [14].

The induced current can be approximated as an image current in a perfectly conducting plane at some arbitrary position in the plasma, such as at half the skin depth from the antenna–plasma interface [19]. Values for L_0, L_2, and their mutual inductance M_{02} can be calculated using expressions for the inductance of linear conductors and the image current method [20]. The impedance of each leg in the presence of plasma inductive coupling is given by the series equivalent circuit in figure 3 where the secondary (plasma) circuit is transformed in terms of the primary circuit current [14, 21]. Finally, the leg impedance $Z_2 = R + j\omega L$ in figure 1 is represented by $R_0 + j\omega L_0$ in the absence of plasma, and $(R_0 + aR_2) + j\omega(L_0 - aL_2 - aR_2/\nu)$ in the presence of plasma inductive coupling [14], where $a = \omega^2 M_{02}^2/[(\omega L_2 +$

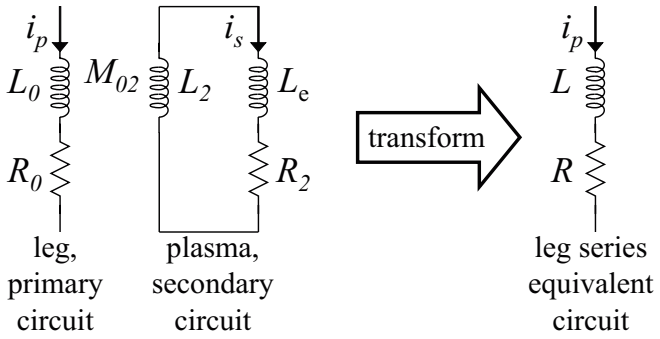

Figure 3. Electrical circuit of the current i_p in the leg (primary circuit: self-inductance L_0, resistance R_0) inductively coupled with the plasma current i_s (secondary circuit: self-inductance L_2, plasma resistance R_2, plasma self-inductance L_e), via their mutual inductance M_{02}. The secondary circuit can be transformed into a series equivalent circuit (total self-inductance L, total resistance R) in terms of the primary circuit current. The notation of [14] is used.

$R_2\omega/\nu)^2 + R_2^2]$ is a transformation factor. Hence the analysis of the antenna network properties can be carried out using the circuit of figure 1, on the understanding that the value of $Z_2 = R + j\omega L$ depends on whether there is plasma or not. Note that inductive coupling to the plasma increases the leg resistance by aR_2, and decreases the leg inductance by $(aL_2 + aR_2/\nu)$. The stringer impedances Z_1 are also transformed by plasma coupling although the effect is relatively small because the stringers are short compared with the legs.

It is interesting to note that the particular case of a linear conductor coupled with a conducting, dissipative medium can also be analyzed by the complex-image method [22–24] which gives a self-consistent calculation of the line impedance in terms of the medium conductivity. There is then no need to assume a perfectly conducting plane at an arbitrary position. However, comparison between the transformer method above and the complex-image method goes beyond the scope of this work.

Estimation of the plasma parameters using the antenna input impedance measurements of figure 2 is considered further in section 5.1. First of all, however, in the following sections it is necessary to calculate the relation between the antenna input impedance and the impedances of the legs and stringers which make up the network [7].

3. Normal modes in ladder networks

In figure 4, $\boldsymbol{I}_n$, $\boldsymbol{M}_n$ and $\boldsymbol{K}_n$ are currents while $\boldsymbol{A}_n$ and $\boldsymbol{B}_n$ denote the potentials at the antenna nodes. Ladder networks are conventionally analysed using a loop current description [5], where the loop current $\boldsymbol{J}_n$ in each section is given by $\boldsymbol{J}_n = \boldsymbol{M}_n = -\boldsymbol{K}_n$, and $\boldsymbol{I}_n = \boldsymbol{J}_n - \boldsymbol{J}_{n-1}$. However, to treat the general case of a dissipative-driven antenna in section 4, we will have to introduce into the circuit analysis the input current $\boldsymbol{i}_{rf}$ driven by the antenna RF power supply. This injection of RF current means that $\boldsymbol{M}_n = -\boldsymbol{K}_n$ does not hold everywhere on the antenna, and so the loop current description cannot be used for the dissipative-driven antenna. For consistent notation throughout this work, we will therefore use $\boldsymbol{K}_n$ and

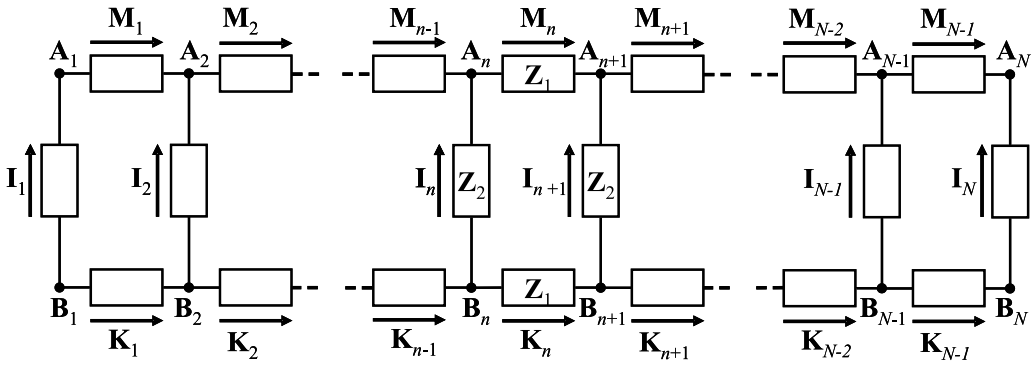

Figure 4. A ladder network segment with N legs made up of stringer impedances $\boldsymbol{Z}_1$ and leg impedances $\boldsymbol{Z}_2$.

$\boldsymbol{M}_n$ instead of loop currents $\boldsymbol{J}_n$. A derivation of the normal mode frequencies and current distributions [5] is now briefly reviewed to introduce the notation and to give a reference point for comparison of the general solution for dissipative antennas in section 4.

3.1. General solution for the leg currents, $\boldsymbol{I}_n$

For the currents and impedances defined in the nth elementary mesh of figure 4, the general set of equations for the circuit analysis is given by Kirchhoff's and Ohm's laws for the currents and voltages,

$$\boldsymbol{M}_n = \boldsymbol{M}_{n-1} + \boldsymbol{I}_n, \tag{1}$$

$$\boldsymbol{K}_n = \boldsymbol{K}_{n-1} - \boldsymbol{I}_n, \tag{2}$$

$$\boldsymbol{Z}_2\boldsymbol{I}_n + \boldsymbol{Z}_1\boldsymbol{M}_n - \boldsymbol{Z}_2\boldsymbol{I}_{n+1} - \boldsymbol{Z}_1\boldsymbol{K}_n = 0. \tag{3}$$

A recurrence relation for the leg currents $\boldsymbol{I}_n$ is obtained by subtracting the voltage equation for the $(n-1)$th mesh and eliminating $\boldsymbol{M}_n$ and $\boldsymbol{K}_n$ using (1) and (2):

$$\boldsymbol{I}_{n+1} - 2\left(1 + \frac{\boldsymbol{Z}_1}{\boldsymbol{Z}_2}\right)\boldsymbol{I}_n + \boldsymbol{I}_{n-1} = 0. \tag{4}$$

The conventional solution is $\boldsymbol{I}_n = \boldsymbol{a}_1\boldsymbol{\Gamma}_1^n + \boldsymbol{a}_2\boldsymbol{\Gamma}_2^n$, where $\boldsymbol{\Gamma}_1$ and $\boldsymbol{\Gamma}_2$ are the roots of the quadratic characteristic equation which can be arranged as

$$\frac{\boldsymbol{\Gamma} + 1/\boldsymbol{\Gamma}}{2} = \left(1 + \frac{\boldsymbol{Z}_1}{\boldsymbol{Z}_2}\right). \tag{5}$$

Recognizing that these roots are reciprocal, we write $\boldsymbol{\Gamma_1} = \mathrm{e}^{-\gamma}$ and $\boldsymbol{\Gamma_2} = \mathrm{e}^{\gamma}$, whereupon the characteristic equation becomes

$$\cosh\gamma = \left(1 + \frac{\boldsymbol{Z}_1}{\boldsymbol{Z}_2}\right), \tag{6}$$

and the general solution for the antenna leg currents is therefore

$$\boldsymbol{I}_n = \boldsymbol{a}_1\mathrm{e}^{-\gamma n} + \boldsymbol{a}_2\mathrm{e}^{\gamma n}, \tag{7}$$

where $\boldsymbol{a}_1$ and $\boldsymbol{a}_2$ are complex constants to be determined from boundary conditions. The solution given by (6) and (7) holds for any impedances $\boldsymbol{Z}_1$ and $\boldsymbol{Z}_2$, and is therefore valid for dissipative antennas also. For harmonic currents with $\mathrm{e}^{\mathrm{j}\omega t}$ time dependence, the leg currents are $\boldsymbol{I}_n\mathrm{e}^{\mathrm{j}\omega t}$ so that the general solution is seen to consist of a forward traveling wave $\boldsymbol{a}_1\exp(\mathrm{j}\omega t - \gamma n)$ and a backward traveling wave $\boldsymbol{a}_2\exp(\mathrm{j}\omega t + \gamma n)$, where $\gamma = \alpha + \mathrm{j}\beta$ is the propagation constant, α is the attenuation constant per section and β is the phase change per section (α and β are both real).

3.2. Normal modes for a non-dissipative planar antenna

For a non-dissipative ladder network, the impedances $\boldsymbol{Z}_1 = 1/(\mathrm{j}\omega C) + \mathrm{j}\omega M$ and $\boldsymbol{Z}_2 = \mathrm{j}\omega L$ are purely imaginary and their ratio in (6) is purely real. The propagation constant then corresponds to $\gamma = \mathrm{j}\beta$ in (6):

$$\cos\beta = 1 + \frac{M}{L} - \frac{1}{\omega^2 LC}. \tag{8}$$

For this special case of a lossless antenna, there is no injection of RF current to consider and so $\boldsymbol{M}_n = -\boldsymbol{K}_n$. Using (1)–(3) gives the same recurrence relation as for $\boldsymbol{I}_n$, hence $\boldsymbol{M}_n = -\boldsymbol{K}_n = \boldsymbol{b}_1\mathrm{e}^{-\mathrm{j}\beta n} + \boldsymbol{b}_2\mathrm{e}^{\mathrm{j}\beta n}$. Recognizing that $\boldsymbol{M}_0 = 0$ from figure 4, we have $\boldsymbol{b}_1 = -\boldsymbol{b}_2$, and the currents $\boldsymbol{M}_n$ in the non-dissipative ladder network are therefore proportional to $\sin(n\beta)$. The finite length condition $\boldsymbol{M}_N = 0$ further implies that $N\beta = m\pi$. When combined with (8), this leads to the existence of normal mode frequencies [5]

$$\omega_m = \frac{1}{\sqrt{C\left(M + 2L\sin^2\left(\dfrac{m\pi}{2N}\right)\right)}}, \quad (m = 1, 2, \ldots, N-1), \tag{9}$$

and imposes the spatial distribution for $\boldsymbol{M}_n$:

$$\boldsymbol{M}_n \propto \sin\left(n\frac{m\pi}{N}\right), \qquad (m = 1, 2, \ldots, N-1), \tag{10}$$

where the phase shift per section $\beta = \frac{m\pi}{N}$ is proportional to the mode number m. The normal mode current in each leg, using (10) in (1), is given by [5]

$$\boldsymbol{I}_n \propto \sin\left(\frac{m\pi}{2N}\right)\cos\left[\left(n - \frac{1}{2}\right)\frac{m\pi}{N}\right], \quad (m = 1, 2, \ldots, N-1). \tag{11}$$

To summarize, a N-leg lossless planar antenna presents $(N-1)$ normal modes [5] whose current amplitudes have sinusoidal spatial distributions and which oscillate in phase.

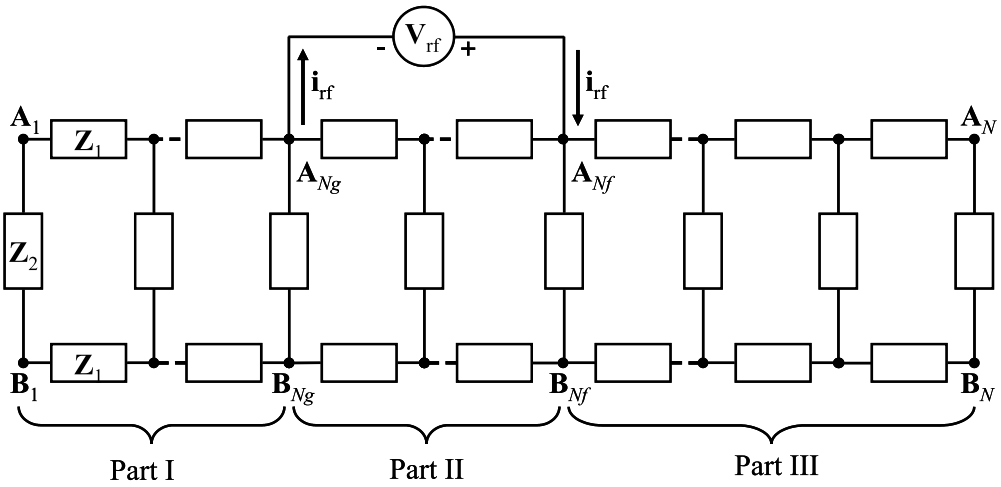

Figure 5. Equivalent circuit of a Helyssen-driven planar antenna showing the three parts I, II, and III. The driving current $i_{\rm rf}$ from the RF power supply is fed into the antenna via node $n = N_{\rm f}$ with the return path via node $N_{\rm g}$. The boundaries between the three parts are defined by the nodes $N_{\rm g}$ and $N_{\rm f}$, where $N_{\rm g} < N_{\rm f}$ in this work.

4. Dissipative networks: Helyssen plasma sources

A real antenna dissipates power due to the electrical resistance of its components. Furthermore, when used as a plasma source, power injected into the antenna is partially transferred to the plasma by coupling to the dissipative medium. The question then arises as to whether the resonance properties of non-dissipative antennas are preserved in the presence of such a coupling to efficiently maintain a well-controlled plasma source. In the following, the resistances R and r are responsible for the power dissipation, and the impedances are now $Z_1 = r + 1/(\mathrm{j}\omega C) + \mathrm{j}\omega M$ and $Z_2 = R + \mathrm{j}\omega L$. For an antenna used as an inductively coupled plasma source, a realistic value for R would not be more than a few ohms (an estimate of $R < 122\,\mathrm{m}\Omega$ is derived in section 5.1).

We define a Helyssen planar resonant antenna as a driven, dissipative ladder network with arbitrary feed-point positions for the RF power connections, as shown in figure 5. This work considers the following points for antenna design:

(i) The values of the antenna input impedance and the antenna components L, R, C, M, r;
(ii) Optimum design of the connection configuration and the choice of mode;
(iii) Estimation of the current and mode perturbations due to the injected rf driving current, and the effect of plasma on the antenna impedance and its component values.

4.1. Current distribution in a dissipative antenna with arbitrary connection configuration

Because of current injection $i_{\rm rf}$ from the RF power supply (figure 5), a single solution for the whole antenna can no longer be found. Instead, separate solutions have to be determined for each part of the antenna, with respect to the boundary conditions at the nodes of current injection.

The total net current along the line is $i_{\rm line} = M_n + K_n$. By adding (1) and (2), $i_{\rm line} = M_n + K_n = M_{n-1} + K_{n-1}$ which is constant along a line segment if not interrupted by current injection nodes. For current continuity, referring to figure 5, $i_{\rm line} = 0$ in parts I and III, and $i_{\rm line} = -i_{\rm rf}$ in part II of the line which carries the RF current circulating via the RF power supply.

For antenna impedance calculations, it will also be necessary to consider the RF voltages A_n and B_n at the antenna nodes in figure 5. The voltages across the antenna impedances, by Ohm's law, are

$$A_n - A_{n+1} = Z_1 M_n, \tag{12}$$

$$B_n - B_{n+1} = Z_1 K_n, \tag{13}$$

$$B_n - A_n = Z_2 I_n. \tag{14}$$

The sum of (12) and (13) is $(A_n + B_n) - (A_{n+1} + B_{n+1}) = Z_1(M_n + K_n)$ from which the sum of voltages at the nth node can be written as

$$A_n + B_n = V_0 - nZ_1 i_{\rm line}, \tag{15}$$

where V_0 is a different constant for each part. Using (14) and (15), the node voltages in terms of the dissipative antenna leg currents I_n are

$$A_n = [V_0 - nZ_1 i_{\rm line} - Z_2 I_n]/2, \tag{16}$$

$$B_n = [V_0 - nZ_1 i_{\rm line} + Z_2 I_n]/2, \tag{17}$$

where $i_{\rm line} = 0$ for parts I and III, and $i_{\rm line} = -i_{\rm rf}$ in part II as above. The stringer currents are then found using (12) and (13):

$$M_n = \left[i_{\rm line} + \frac{Z_2}{Z_1}(I_{n+1} - I_n) \right]/2, \tag{18}$$

$$K_n = \left[i_{\rm line} - \frac{Z_2}{Z_1}(I_{n+1} - I_n) \right]/2, \tag{19}$$

where it can be seen that, in part II of the antenna, the circulating RF current $i_{\rm line} = -i_{\rm rf}$ is shared equally between the two stringers of the antenna.

The solution for the currents in the dissipative antenna is shown in appendix A, and figure 6 shows the calculated current

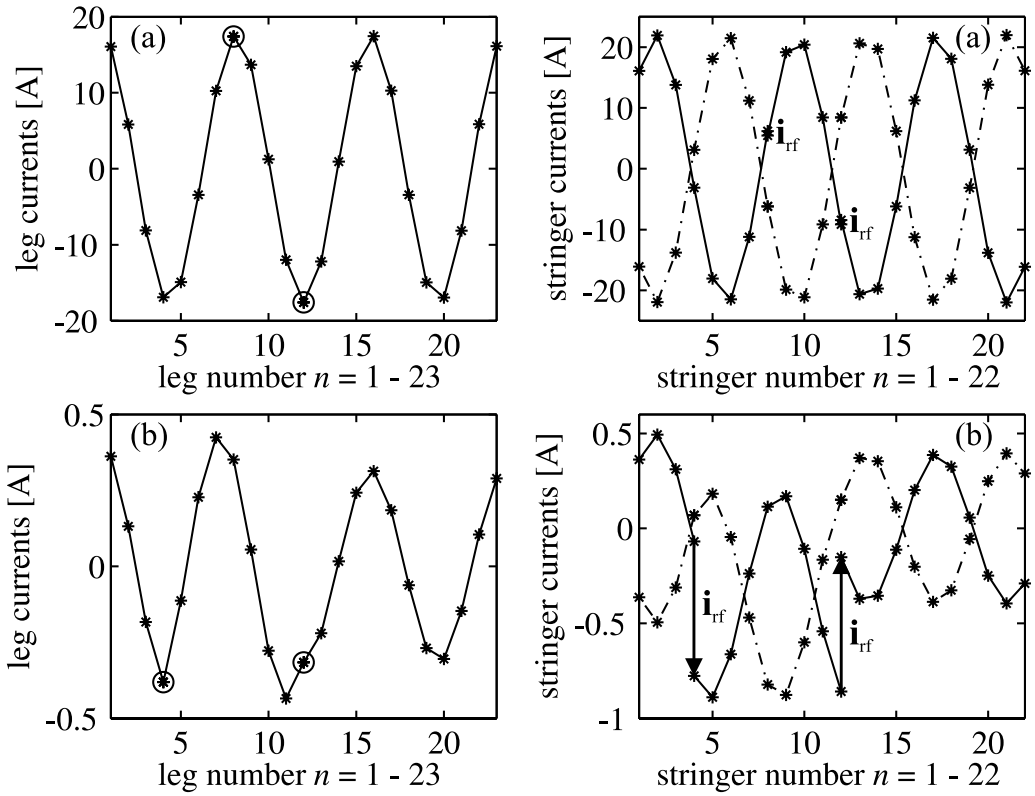

Figure 6. Driven RF currents in a dissipative antenna calculated for RF connection points $N_f = 12$ and (*a*) $N_g = 8$, or (*b*) $N_g = 4$. Left: leg currents $\boldsymbol{I}_n$, where the RF connection positions are marked by circles. Right: stringer currents, full line $\boldsymbol{M}_n$, dashed line $\boldsymbol{K}_n$. Representative experimental antenna component values: $N = 23$ legs, $L = 143$ nH, $R = 36$ mΩ, $C = 2.6$ nF, $M = 7.9$ nH, $r = 2$ mΩ. Mode $m = 6$, at time $\exp(j\omega t) = \exp(j\pi/4)$ for RF current $|\boldsymbol{i}_{rf}| = 1$ A.

distribution in the legs and stringers of a dissipative antenna corresponding to an experimental arrangement [2, 3]. Two cases are shown: (*a*) for feed-points $(N_g, N_f) = (8, 12)$ where the antenna resonant currents are much larger than $\boldsymbol{i}_{rf}$; and (*b*) for feed-points $(N_g, N_f) = (4, 12)$ where $\boldsymbol{i}_{rf}$ is comparable to the antenna currents. The arrows in (*b*) mark the differences in the $\boldsymbol{M}_n$ currents at nodes N_g and N_f which arise to respect current continuity with the RF current injection. From the point of view of current uniformity, it is clearly necessary to arrange for the RF input current to be as small as possible compared with the antenna currents.

At resonance, in the limit of weak dissipation, $\alpha \to 0$, the current distributions (A.1)–(A.3) in all three parts tend towards the same limit (see section B.1 in the appendix):

$$\left(\frac{\boldsymbol{I}_n}{\boldsymbol{i}_{rf}}\right)_{\alpha\to 0} \simeq \left(\frac{j}{\alpha N}\right) \cdot \sin\left(\frac{m\pi}{2N}\right) \cos\left[\left(n-\frac{1}{2}\right)\frac{m\pi}{N}\right] \cdot \left[\frac{D}{\cos\left(\frac{m\pi}{2N}\right)}\right], \tag{20}$$

$$D = \cos\left[\left(N_g-\frac{1}{2}\right)\frac{m\pi}{N}\right] - \cos\left[\left(N_f-\frac{1}{2}\right)\frac{m\pi}{N}\right]. \tag{21}$$

The first bracket of (20) shows that the RF driving current $\boldsymbol{i}_{rf}$ is in phase quadrature ($j = e^{i\pi/2}$) with respect to the leg currents $\boldsymbol{I}_n$. The inverse dependence on α means that the driving current becomes negligible compared with the leg currents, $|\boldsymbol{i}_{rf}| \ll |\boldsymbol{I}_n|$, in the limit of a lossless antenna, i.e. a non-zero resonant current persists as the driving current tends to zero. The (sin, cos) product in (20) shows that the normal mode current distribution (11) is recovered for a weakly dissipative antenna. Also, the amplitude of the spatial distribution of leg currents becomes uniform along all three parts of the antenna in the normal mode limit $\alpha \to 0$ because the driving current $\boldsymbol{i}_{rf}$ becomes negligible compared with $\boldsymbol{I}_n$. The factor D in (20) accounts for the choices of mode number m and of RF current injection connections (N_g, N_f). When the injection points coincide with a maximum and a minimum in the leg currents, as for $(N_g, N_f) = (8, 12)$ in figure 6(*a*), the RF excitation is efficiently coupled to the antenna resonant current distribution, then $|\boldsymbol{I}_n/\boldsymbol{i}_{rf}| \gg 1$, and $|D| = 1.99$ is close to its maximum of 2. Conversely, when the RF connections positions do not correspond to the normal mode spatial variation of the leg currents, as for $(N_g, N_f) = (4, 12)$ in figure 6(*b*), the driven currents $\boldsymbol{I}_n$ are not large compared with the RF current, and $|D| = 0.037$ is close to zero. The importance of D for the antenna input impedance is described in section 4.3.

4.2. Input impedance of a dissipative antenna

The input impedance of a Helyssen antenna determines the required level of driven RF current for a given power injection, and determines the parameters necessary for matching the antenna to the power source output impedance. In figure 5, the RF voltage, $\boldsymbol{V}_{rf}$, across the input nodes is given by $\boldsymbol{A}_{N_f} - \boldsymbol{A}_{N_g}$.

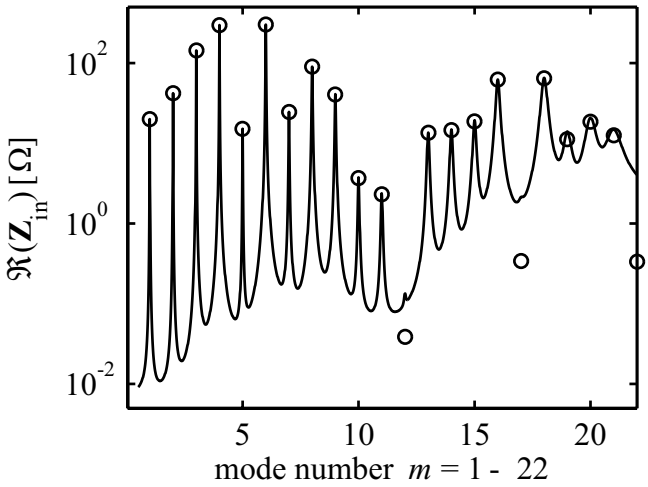

Figure 7. Real input impedance as a function of mode number for the same antenna component values as in figure 6. RF connections $(N_g, N_f) = (8, 12)$. Lines using the exact expression (23); points using the approximation (27).

From (16),

$$\boldsymbol{V}_{rf} = \left[\boldsymbol{Z}_1(N_f - N_g)\boldsymbol{i}_{rf} - \boldsymbol{Z}_2(\boldsymbol{I}_{N_f} - \boldsymbol{I}_{N_g})\right]/2. \tag{22}$$

The exact expression for the antenna input impedance $\boldsymbol{Z}_{in} = \boldsymbol{V}_{rf}/\boldsymbol{i}_{rf}$ follows directly using (A.2) to give

$$\boldsymbol{Z}_{in} = \frac{\boldsymbol{Z}_1}{2}(N_f - N_g) + \boldsymbol{Z}_2\boldsymbol{F}_{(\gamma,N)}\boldsymbol{G}, \tag{23}$$

where $\boldsymbol{F}_{(\gamma,N)}$ is given by (A.4), and $\boldsymbol{G}_{(\gamma,N_g,N_f,N)}$ is a form factor which accounts for the influence of the general configuration of the RF connection positions:

$$\begin{aligned}\boldsymbol{G} = {} & (\cosh\gamma(N - 2N_f + 1) + \cosh\gamma(N - 2N_g + 1))/2 \\ & + \cosh\gamma N - \cosh\gamma(N - N_g - N_f + 1) \\ & - \cosh\gamma(N + N_g - N_f).\end{aligned} \tag{24}$$

The first term of the impedance expression (23) is the parallel combination of the two rows of $(N_f - N_g)$ impedances $\boldsymbol{Z}_1$ between the RF driving current connections. The second term, proportional to $\boldsymbol{Z}_2$, is periodic in mode number (and frequency) and is responsible for the series of peaks in the real input impedance shown in figure 7. The input impedance $\boldsymbol{Z}_{in}$ in (23) is exact for any values of component impedances $\boldsymbol{Z}_1$, $\boldsymbol{Z}_2$, hence for any level of dissipation, and for the continuous range of frequencies.

The characteristic equation (6) for the dissipative antenna, using $\boldsymbol{Z}_1 = r + 1/(\mathrm{j}\omega C) + \mathrm{j}\omega M$ and $\boldsymbol{Z}_2 = R + \mathrm{j}\omega L$, is now

$$\cosh\gamma \simeq \left[1 + \frac{M}{L} - \frac{1}{\omega^2 LC}\right] - \mathrm{j}\left[\frac{R'}{\omega^3 L^2 C}\right], \tag{25}$$

$$R' \simeq R\left[1 - \omega^2 MC\left(1 - \frac{r}{R}\frac{L}{M}\right)\right], \tag{26}$$

where R' is the combined effective resistance of R and r, and small resistances are assumed. By expanding $\cosh\gamma = (\cosh\alpha)(\cos\beta) + \mathrm{j}(\sinh\alpha)(\sin\beta)$ and equating real parts, we again find (8), to first order in the small quantity α, since then $\cosh\alpha \simeq 1$ (see section B.1 in the appendix). Hence the impedance peaks of the weakly dissipative antenna are at almost the same frequencies as the normal mode frequencies (9). The values of R and r therefore do not alter the resonance frequencies to first order in α, which is a useful property for the case of purely resistive loading due to plasma dissipation, because a fixed RF driving frequency can be used.

In the limit of weak dissipation, the real and imaginary parts of the antenna input impedance at the resonance of mode m can be approximated by (see section B.1 in the appendix):

$$\Re(\boldsymbol{Z}_{in}^{res}) \simeq \frac{\omega_m^2 L^2}{R'}(1 - w_m^2 MC)\frac{D^2}{2N}, \tag{27}$$

$$\Im(\boldsymbol{Z}_{in}^{res}) \simeq \frac{(N_f - N_g)}{2}\left[\omega_m M - \frac{1}{\omega_m C}\right], \tag{28}$$

where $0 \leqslant D^2 \leqslant 4$, using (21). In figure 7, (27) gives a good approximation to the real part of the exact expression (23) at resonance for values above 1 Ω.

4.3. Optimization of the input impedance by choices of mode number and RF connection positions

The antenna input impedance is influenced by the mode number m and the RF connection positions (N_g, N_f). A high input impedance is necessary to minimize the RF injection current for a given power so that the antenna current sinusoidal distribution is as uniform as possible along the antenna.

The scaling of the antenna real input impedance is given by (27). For maximizing the real impedance, there is a general trend for high mode frequency ω_m (low mode number) and low leg resistance R, which is strongly modulated by the connection configuration term, D^2, from (21).

Figure 8 represents a mapping of the antenna real input impedance $\Re(\boldsymbol{Z}_{in})$ in the (N_g, N_f) plane for mode $m = 6$. This is a graphical demonstration of the impedance modulation which is approximately proportional to D^2. Once the number of legs N and the mode number m are chosen, the value of D^2 depends only on the antenna connection positions (N_g, N_f). For each mode, the connection positions can be chosen to obtain a value close to the maximum, $D^2 \simeq 4$. For example, in figure 8, $D^2 = 3.96$ for $(N_g, N_f) = (8, 12)$ for which the real input impedance is close to the maximum 302 Ω, but $D^2 = 0.0014$ for $(N_g, N_f) = (4, 12)$ for which the real input impedance is only 0.13 Ω.

The choice of (N_g, N_f) is therefore a design parameter for the real input impedance of the driven antenna. To minimize the reactive component of the antenna input impedance at resonance, the connections should be as close together as possible (respecting $D^2 \approx 4$) to give the lowest value of $(N_f - N_g)$ according to (28).

Finally, for all the resonant modes, the peak values of real input impedance are approximately inversely proportional to the effective resistance R', as shown by (27) and figure 9. When the antenna sustains a plasma, the dissipation due to the plasma load will increase the value of the antenna resistances, and consequently reduce the antenna input impedance. This is important in terms of RF power injection because it

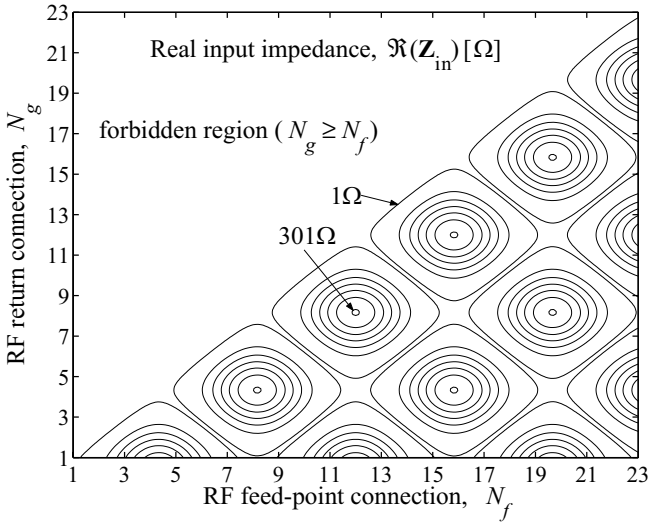

Figure 8. Contour plot of the real part of the antenna input impedance, $\Re(\boldsymbol{Z}_{\rm in})$, using (23) for continuum ranges of $N_{\rm g}$ and $N_{\rm f}$. The relevant values of real input impedance correspond to integer values of $(N_{\rm g}, N_{\rm f})$. The contours are from 301 Ω (the innermost circles) down to 1 Ω in 50 Ω intervals. Mode $m = 6$, and the same antenna component values as for figure 6.

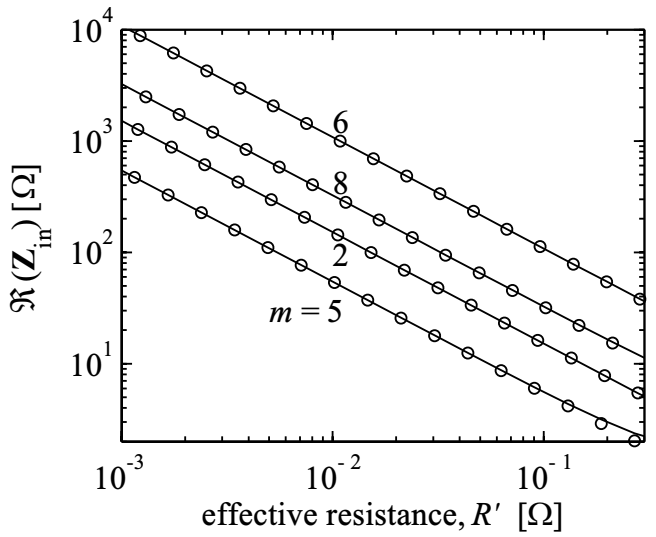

Figure 9. The real input impedance at resonance as a function of the effective resistance R', for modes $m = 2, 5, 6, 8$. Lines using the exact expression (23); points using the approximation (27). Connection positions $(N_{\rm g}, N_{\rm f}) = (8, 12)$; antenna component values as for figure 6.

means that the conditions for impedance matching between a load and a RF generator with 50 Ω output impedances can already be almost fulfilled. In contrast, conventional large-area RF plasma sources, capacitively or inductively coupled, present almost purely imaginary input impedances which tend towards zero or very high values, respectively, with increasing source area.

4.4. Antenna input current for constant power injection

We now consider the RF current in a dissipative planar antenna for a given RF power input $P_{\rm rf}$. An approximate scaling law for the driving RF current amplitude $\hat{i}_{\rm rf} = |\boldsymbol{i}_{\rm rf}|$ is obtained from $P_{\rm rf} = \Re(\boldsymbol{Z}_{\rm in}^{\rm res})(\hat{i}_{\rm rf})^2/2$ and (27) so that

$$\hat{i}_{\rm rf} \simeq \frac{2}{\omega_m L|D|}\sqrt{\frac{P_{\rm rf} N R'}{(1 - w_m^2 MC)}}. \qquad (29)$$

The RF current for a given power is minimized for optimum connection configurations having the maximum value $|D| = 2$.

As an example, figure 10 shows the dependence of $\hat{i}_{\rm rf}$ on the leg resistance R for different positions $N_{\rm g}$ of the RF return connection, with $N_{\rm f} = 12$. According to figure 8, the antenna input impedance is maximized by choosing $N_{\rm g} = 8$. Therefore, at fixed input power, the input current is lower for $N_{\rm g} = 8$ than for all other ground connections in figure 10.

4.5. Perturbations to the normal mode phase distribution due to the RF driving current

The properties of normal modes, such as a uniform sinusoidal distribution of the leg currents along the antenna, and phase equality of all the oscillating leg currents, are ideal for using the antenna as a uniform plasma source. However, the injection of the RF driving current $\boldsymbol{i}_{\rm rf}$ is also a perturbation to the normal

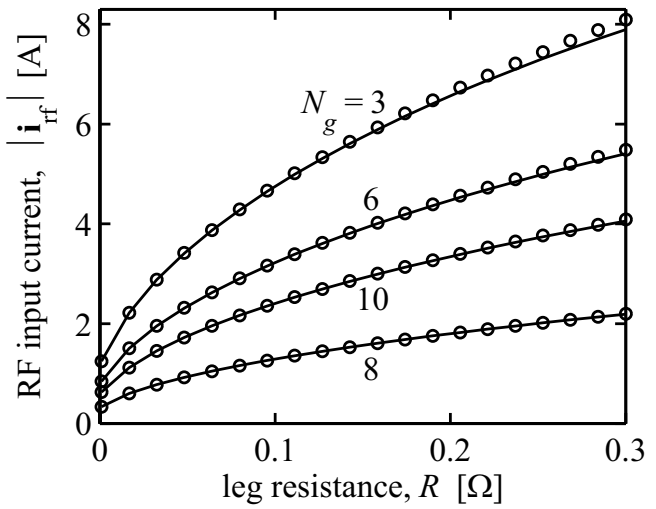

Figure 10. Amplitude of the input current $\hat{i}_{\rm rf}$ at 100 W RF power, as a function of leg resistance, for ground connections $N_{\rm g} = 3$, 6, 8 and 10, with $N_{\rm f} = 12$ and mode $m = 6$. Lines using the exact expression (23); points using the approximation (27). Antenna component values as for figure 6.

mode phase distribution because of its non-zero amplitude and its phase quadrature (see (20)) relative to the antenna currents. Figure 11 shows the leg currents as a function of time, $I_n(t)$, and their phase ϕ_n relative to the RF current, using (A.1) to (A.3), where $\boldsymbol{I}_n = \hat{I}_n \exp(\mathrm{j}\phi_n)$.

Figure 11(a) corresponds to a quasi-non-dissipative antenna ($R = 36\,\mathrm{m}\Omega$) with optimum connection positions $(N_{\rm g}, N_{\rm f}) = (8, 12)$ excited at its $m = 6$ resonance frequency with RF current $\hat{i}_{\rm rf} = 1$ A. The leg currents are temporally in phase and their amplitude follows the sinusoidal distribution expected according to the normal mode expressions (11).

Figure 11(b) shows the perturbation to the current phase equality for higher leg resistance $R = 1\,\Omega$: The more resistive the antenna legs, the lower the input impedance (see (27)),

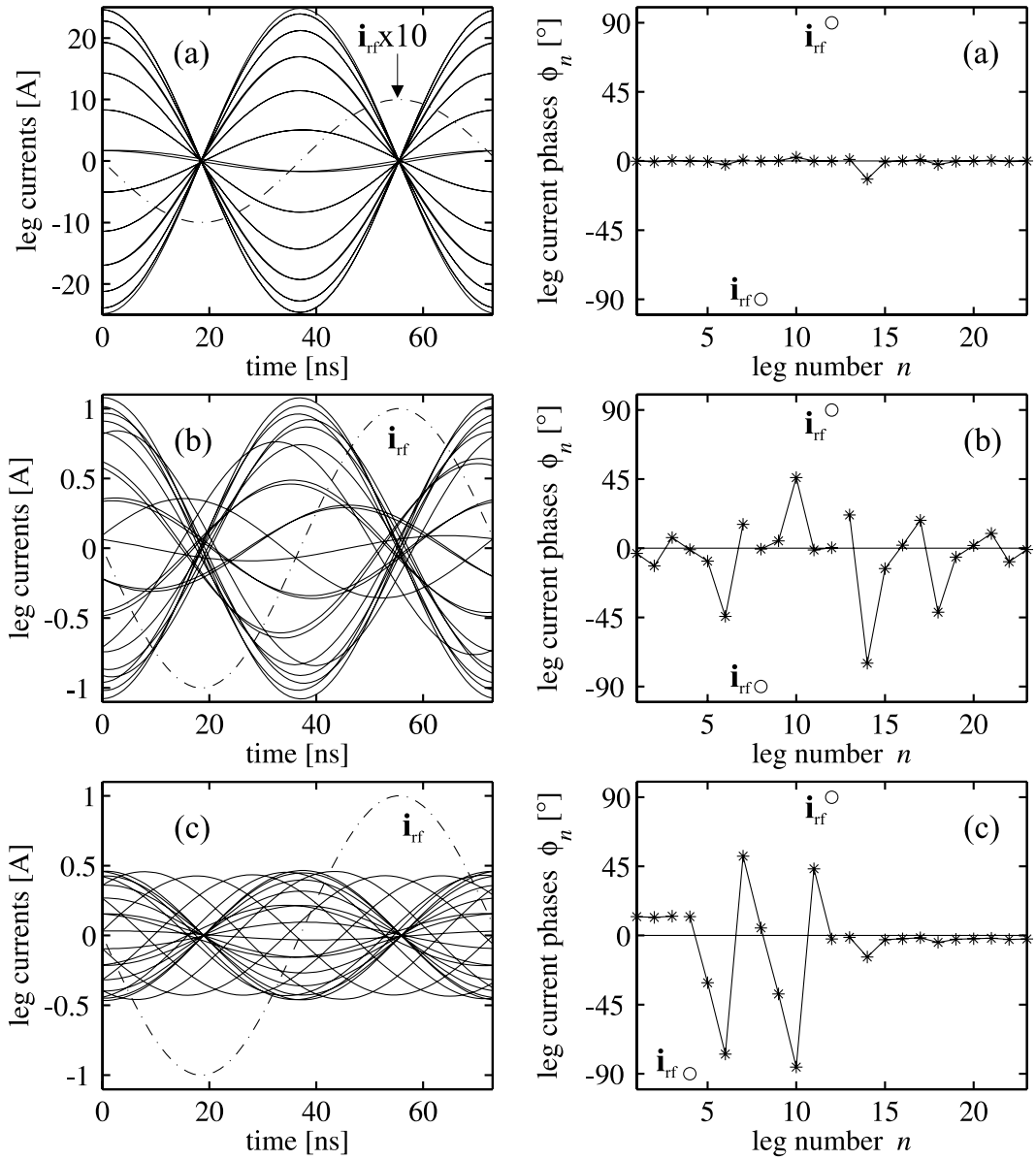

Figure 11. Left: currents in all the antenna legs, and the RF current, as a function of time for one RF period at 13.56 MHz. Right: their phases referenced to the RF feed-point driving current at 90°, for $\hat{i}_{rf} = 1$ A. (*a*) Optimum connections (N_g, N_f) = (8, 12) and low leg resistance $R = 36\,\text{m}\Omega$; (*b*) optimum connections but high leg resistance, $R = 1\,\Omega$; (*c*) low leg resistance ($R = 36\,\text{m}\Omega$) but non-optimum connections (N_g, N_f) = (4, 12). The phases for the RF driving current are labelled by $\boldsymbol{i}_{rf}$. Mode $m = 6$, with antenna component values as for figure 6 unless otherwise stated.

and the lower the leg currents with respect to the RF current. The equivalent circuit approach in section 5 will be used to estimate the increase in the effective leg resistance due to plasma loading.

Figure 11(*c*) shows the effect of the connection configuration D on the phase equality of the antenna currents by changing the ground connection position to $N_g = 4$. The current phase equality is strongly perturbed even though the leg resistance has the same low value as for figure 11(*a*). The perturbed distribution is due to the low input impedance associated with the $N_g = 4$ feeding configuration.

Since dissipative coupling to the plasma increases the value of R, it is all the more important that the connection configuration be chosen so that $D^2 \simeq 4$ to obtain the maximum value of the real input impedance. In terms of plasma generation, situations (*b*) and (*c*) would cause non-uniformities in heating and electron density. To maintain the amplitude uniformity and phase equality of normal modes, it is therefore necessary that the leg current amplitude be as large as possible compared with the RF current, which is obtained for high input impedance.

5. Parallel resonance approximation for the input impedance near to a resonance frequency

In the neighborhood of a resonance frequency, each peak in figure 7 has a form similar to the parallel resonance behavior measured experimentally [2] with and without plasma, as

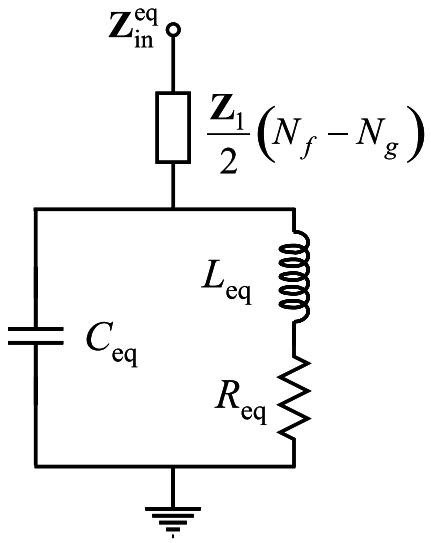

Figure 12. An equivalent circuit, in the neighborhood of a mode resonance, for the dissipative antenna shown in figure 5 with the components of figure 1. Using (30) to (35), this circuit accounts for all the antenna components L, R, C, M, r, the mode number m, and general RF connection positions (N_{g}, N_{f}).

shown in figure 2. A model of the antenna impedance is useful to understand how the individual antenna components are related to the equivalent parallel resonance circuit parameters which can be conveniently measured. The effect of plasma loading on the antenna can then be deduced from the equivalent circuit parameters.

To interpret the antenna impedance behavior close to resonance, we consider an approximation for $\boldsymbol{Z}_{\text{in}}$ by expansion of (23) in terms of a small deviation dω from a resonance frequency ω_m (see section B.2 in the appendix). It is found that the input impedance (23) of the dissipative antenna in the neighborhood of the mth mode resonance can be represented by an impedance $\boldsymbol{Z}_1(N_{\text{f}}-N_{\text{g}})/2$ in series with a parallel resonance equivalent circuit, as shown in figure 12. The equivalent circuit parameters are as follows:

$$\boldsymbol{Z}_{\text{in}}^{\text{eq}} \simeq \frac{\boldsymbol{Z}_1}{2}(N_{\text{f}} - N_{\text{g}}) + \frac{1}{\boldsymbol{Y}_{\text{eq}}}, \tag{30}$$

$$\boldsymbol{Y}_{\text{eq}} = \frac{1}{R_{\text{eq}}Q^2}\left[1 + \text{j}2Q\frac{\text{d}\omega}{\omega_m}\right], \tag{31}$$

$$R_{\text{eq}} = R'(1 - \omega_m^2 MC)\frac{D^2}{2N}, \tag{32}$$

$$L_{\text{eq}} = L(1 - \omega_m^2 MC)\frac{D^2}{2N}, \tag{33}$$

$$Q = \omega_m L_{\text{eq}}/R_{\text{eq}} = \omega_m L/R', \tag{34}$$

$$C_{\text{eq}} = \frac{C\,[1 - \cos(m\pi/N)]}{(1 - \omega_m^2 MC)^2}\frac{2N}{D^2}. \tag{35}$$

The values of R_{eq}, L_{eq}, C_{eq} can be uniquely determined for each mode number m by measuring the antenna impedance in the neighborhood of the mth resonance. The angular frequency at resonance, $\omega_m = 1/\sqrt{L_{\text{eq}}C_{\text{eq}}}$, is the same expression as for the normal mode resonance in (9). Also, the real input impedance at resonance of the equivalent circuit, $R_{\text{eq}}Q^2$, is identical to the previous expression (27). The quality factor Q of the equivalent circuit represents the Q factor of the whole antenna system [5]: it is given in terms of the antenna individual components L, R, C, M, r and the mode number m using (34) and (26). Once the series impedance $\boldsymbol{Z}_1(N_{\text{f}}-N_{\text{g}})/2$ is accounted for, Q is in fact independent of the RF connection positions. The equivalent circuit approximation is indistinguishable from the exact impedance (23) for the conditions in figure 2.

5.1. The measured effect of plasma excitation on the antenna impedance

Figures 2(a) and (b) show the antenna impedance measured around mode $m = 6$ without plasma, and with plasma, respectively [2]. The fitted parameters (C_{eq}, L_{eq}, R_{eq}) are (13.13 nF, 10.55 nH, 2.65 mΩ) without plasma, and (15.09 nF, 9.166 nH, 6.68 mΩ) with plasma. The impedance of the resonant antenna can easily be measured with sufficient accuracy using voltage and current probes, in contrast to the highly reactive impedance of capacitive or inductive reactors where a small error in the phase difference between voltage and current near $\pm 90^\circ$ results in large errors. The antenna input impedance at resonance decreases strongly from 302 to 90 Ω when the plasma is excited. In contrast, the 13.525 MHz antenna resonance frequency increases by only about 7 kHz in the presence of plasma: for this experimental situation, it is found that the measured relative changes in L_{eq} and C_{eq} are such that their product, and thus $\omega_m = 1/\sqrt{L_{\text{eq}}C_{\text{eq}}}$, remains almost the same when the plasma is excited. As a first step to understanding the coupling between antenna and plasma [14, 16, 25], the effect of the plasma on the antenna component values L, R, C, M, r will now be calculated from the parallel resonance measurements C_{eq}, L_{eq}, R_{eq} using the antenna equivalent circuit model above.

For analysis in terms of the antenna components, C is taken to be a constant equal to the capacitor's nominal value, $C = 2.6$ nF, since the plasma sheath capacitive coupling is not expected to be more than a few pF. The capacitances C built into the resonant antenna are, in fact, much larger than the small parasitic capacitances found in conventional coil antennas used for inductively coupled plasma sources. For $N = 23$ legs and RF connections (N_{g}, N_{f}) = (8, 12), the value of $D^2 = 3.96$ is close to optimum. Using (30)–(35) it is now possible to calculate the antenna component values:

(i) Without plasma, at resonance frequency 13.525 MHz, the calculated inductances $M = 7.9$ nH, from (35), and $L = 143$ nH, from (33), are in reasonable agreement with the experimental component estimations [2], 6 nH and 156 nH respectively. The calculated range of the leg resistance is $36 < R < 42$ mΩ, using (26) and (32), depending on whether the resistances r, R are in proportion to their associated inductances M, L, respectively (so that $\frac{r}{R}\frac{L}{M} = 1$, whereupon $r = 2$ mΩ), or negligibly small ($r = 0$). These were used as the example parameters throughout this work, as given in the caption of figure 6(a).

(ii) With plasma, at resonance frequency 13.532 MHz, the calculated inductances are now $M = 10.7$ nH and $L = 134$ nH. The calculated range of the leg resistance is $97 < R < 122\,\mathrm{m\Omega}$, again depending on how r is estimated. The strong increase in resistance R due to plasma loading (see figure 3 and accompanying text) is not so large as to perturb the phase equality of the leg currents. The leg inductance L has diminished by 9 nH, whereas the small inductance M is estimated to increase by almost 3 nH. The error is estimated to be not more than 1 nH for both inductances. On the basis of this model, the increase in M in (35) accounts for the measured increase in C_{eq} which is responsible for the almost-unchanged resonance frequency when the plasma is excited. The decrease in L could be interpreted as the consequence of inductive coupling between the antenna and the plasma [14, 16, 25] as discussed in section 2. However, the apparent increase in M cannot be understood on this basis since plasma inductive coupling would be expected to decrease the inductance of all conducting elements. In fact, the observed frequency shift is not only determined by inductive coupling to the plasma but also by the partial screening by the plasma of the mutual inductances between the legs [7]. The estimations of changes in resistance and inductance remain valid, but an analysis of plasma parameters based on section 2 and antenna input impedance measurements would require knowledge of the inductance change due to transformer coupling, separately from the mutual impedance effect. However, the consideration of mutual inductances is beyond the scope of this paper. The real input impedances with and without plasma, calculated at resonance using (27) or $R_{\mathrm{eq}}Q^2$, are consistent with the measured values.

To summarize, the dominant effect of plasma excitation on the antenna is to triple the effective resistance of its legs. This is due to antenna coupling with the dissipative plasma. For this example, the measured resonance frequency remains almost the same when the plasma is excited, due to changes in the antenna inductances on the basis of this model. For use as an industrial plasma source [4], this is convenient because a fixed frequency RF power generator can be used, and the dominantly real input impedance near to antenna resonance avoids strong reactive currents and voltages in the RF power feeding which presents problems for conventional large-area plasma sources. However, it remains difficult to understand the details of antenna inductive coupling to the plasma with this first modeling approach: for this, other mode frequencies will have to be investigated, including an analysis of the mutual inductances between the antenna elements [5].

6. Conclusions

A theoretical analysis of Helyssen resonant antennas is presented to aid antenna design for its development as a plasma source for industrial applications. Analytical expressions are given for the leg currents and the input impedance for arbitrary antenna impedances, and for any level of dissipation. Approximations are given for the case of a weakly dissipative high-pass antenna to provide simple scaling laws. The antenna can be represented by a simple equivalent circuit which includes a parallel resonance circuit as shown by experiments with and without plasma. Measurements of the equivalent circuit during plasma excitation were interpreted in terms of the antenna component values. Inductive coupling to the dissipative plasma tripled the leg effective resistance, whereas the resonant frequency was almost unchanged in this case: the change in resonant frequency depends on both plasma inductive coupling and on plasma screening of mutual inductances, which is more difficult to interpret than the increase in effective resistance due to power dissipation in the plasma.

To design a planar antenna for an inductively coupled plasma source, it was shown that a high input impedance is necessary to maintain the current amplitude uniformity and phase equality which are the desirable properties of normal modes. This can be achieved by optimal choice of RF connection positions for a given mode number in a weakly dissipative antenna. The dominantly real input impedance near to antenna resonance avoids the problem of strong reactive currents and voltages in the matching box and RF power connections found in conventional large-area plasma sources. Further improvements to the model will require consideration of mutual inductances.

Acknowledgments

The authors thank M Chesaux for many useful comments. This work was supported by Swiss Commission for Technology and Innovation grant no 9896.2 PFIW-IW.

Appendix A. The currents in the three parts of the antenna

The solution for the currents in the dissipative antenna is obtained by finding the constants $\boldsymbol{a}_1$ and $\boldsymbol{a}_2$ for the currents $\boldsymbol{I}_n$ in (7) for each part of the antenna. These six constants are found using the boundary conditions at both ends (as in section 3.2) and with respect to current continuity between the different parts at nodes $n = N_{\mathrm{g}}$ and $n = N_{\mathrm{f}}$. After some algebra, the leg currents for the general configuration of figure 5 are

$$\boldsymbol{I}_n^{\mathrm{I}} = \boldsymbol{i}_{\mathrm{rf}}\boldsymbol{F}_{(\gamma,N)}\left[\cosh\boldsymbol{g}_1 + \cosh\boldsymbol{g}_{2a} - \cosh\boldsymbol{g}_3 - \cosh\boldsymbol{g}_{4a}\right], \tag{A.1}$$

$$\boldsymbol{I}_n^{\mathrm{II}} = \boldsymbol{i}_{\mathrm{rf}}\boldsymbol{F}_{(\gamma,N)}\left[\cosh\boldsymbol{g}_1 + \cosh\boldsymbol{g}_{2b} - \cosh\boldsymbol{g}_3 - \cosh\boldsymbol{g}_{4a}\right], \tag{A.2}$$

$$\boldsymbol{I}_n^{\mathrm{III}} = \boldsymbol{i}_{\mathrm{rf}}\boldsymbol{F}_{(\gamma,N)}\left[\cosh\boldsymbol{g}_1 + \cosh\boldsymbol{g}_{2b} - \cosh\boldsymbol{g}_3 - \cosh\boldsymbol{g}_{4b}\right], \tag{A.3}$$

$$\boldsymbol{F}_{(\gamma,N)} = \frac{\tanh(\gamma/2)}{2\sinh(\gamma N)}, \tag{A.4}$$

where the arguments of the cosh functions

(i) $\boldsymbol{g}_1 = \gamma(n - 1 + N_{\mathrm{g}} - N)$,
(ii) $\boldsymbol{g}_{2a} = \gamma(n - N_{\mathrm{g}} + N)$,
(iii) $\boldsymbol{g}_{2b} = \gamma(n - N_{\mathrm{g}} - N)$,

(iv) $g_3 = \gamma(n - 1 + N_f - N)$,
(v) $g_{4a} = \gamma(n - N_f + N)$,
(vi) $g_{4b} = \gamma(n - N_f - N)$,

represent the influence of the chosen RF connection positions (N_g, N_f). From (A.1)–(A.3) it can be seen that the current flow in each element of a dissipative antenna is proportional to the driving current i_{rf}, varies non-linearly with γ (via $\boldsymbol{F}$), and depends on the RF connection positions. The importance of these three factors for the antenna input impedance, the antenna currents, and their phases is discussed in sections 4.2–4.4.

Appendix B. Approximations by expansion in the small term α

B.1. Approximations at resonance

The factor $\boldsymbol{F}_{(\gamma,N)}$, defined in (A.4), is used for the leg currents (A.1)–(A.3) and the input impedance (23). For the limit of small attenuation per section, $\alpha \ll 1$, the numerator $\tanh(\gamma/2) \simeq \tanh(j\beta/2) = j\tan(\beta/2)$. In the denominator, $\sinh(\gamma N)$ can be expanded as $\sinh(\alpha N)\cos(\beta N) + j\cosh(\alpha N)\sin(\beta N)$ and since $\sin(\beta N) = \sin(m\pi) = 0$ for normal modes, we have $\sinh(\gamma N) \simeq \alpha N(-1)^m$ for $\alpha N \ll 1$. One expression for $\boldsymbol{F}_{(\gamma,N)}$ at resonance is therefore

$$\boldsymbol{F}^{\text{res}}_{(\gamma,N)} \simeq \frac{j\tan\left(\dfrac{m\pi}{2N}\right)}{2(-1)^m \alpha N}. \tag{B.1}$$

Expansion of the sums of four cosh terms in (A.1)–(A.3) in the limit of small α gives $2(-1)^m \cos[(n - \frac{1}{2})\frac{m\pi}{N}]D$ for all three of the sums. Taking the product with (B.1) gives the normal mode approximation for the current distribution in (20).

$\boldsymbol{F}^{\text{res}}_{(\gamma,N)}$ can also be expressed in terms of L, R, C, M, r by expanding the characteristic equation as in (25). Equating real parts gives $\cos\beta \simeq [1 + \frac{M}{L} - \frac{1}{\omega_m^2 LC}]$ at resonance, and equating imaginary parts gives

$$\alpha \sin\beta \simeq -\frac{R'}{\omega^3 L^2 C}, \tag{B.2}$$

for $\alpha \ll 1$ so that $\cosh\alpha \approx 1$. For the example parameters in the caption of figure 6(*a*), $\alpha = 0.0015$ and $\cosh\alpha = 1$, to 6 decimal places. Using $\tan\frac{\beta}{2} \equiv (1 - \cos\beta)/\sin\beta$ in (B.1) gives the alternative expression

$$\boldsymbol{F}^{\text{res}}_{(\gamma,N)} \simeq \frac{-j\omega_m L(1 - w_m^2 MC)}{2(-1)^m N R'}, \tag{B.3}$$

at resonance. In the expression for the input impedance (23), expansion of the cosh terms in $\boldsymbol{G}$ for small α gives $(-1)^m D^2$. In the limit of weak dissipation, $\boldsymbol{Z}_2 \simeq j\omega L$ and hence the input impedance (23) at resonance can be approximated by (27) for the real part and (28) for the imaginary part.

B.2. Approximations near to resonance

Normal modes excited in a lossless antenna present a discrete frequency spectrum whereas driven currents in a dissipative antenna exhibit a continuous spectrum, with peaks of real impedance at the normal mode resonance frequencies to first order in α (see (25)). For a dissipative antenna, therefore, the mode frequency has continuous values and we consider a small variation in angular frequency $d\omega$ about ω_m, so that $\omega = \omega_m + d\omega$. This corresponds to a mode variation dm about mode number m (where $dm \ll 1$). Whereas $\sin(\beta N) = \sin(m\pi) = 0$ for normal modes, we now have $\sin(\beta N) = \sin[(m + dm)\pi] = \cos(m\pi)\sin(\pi\, dm) \simeq (-1)^m \pi\, dm$ in the proximity of mode m. Expansion of $\sinh(\gamma N)$ now gives

$$\sinh(\gamma N) \simeq (\alpha N + j\pi\, dm)(-1)^m \tag{B.4}$$

in the immediate neighborhood of the mth resonance, for $\alpha N \ll 1$. We now consider

$$\frac{1}{\boldsymbol{F}^{\text{eq}}_{(\gamma,N)}} = \frac{2\sinh(\gamma N)}{\tanh(\gamma/2)} \simeq \frac{2(-1)^m[(\alpha\sin\beta)N + j(\sin\beta)\pi\, dm]}{j(1 - \cos\beta)}, \tag{B.5}$$

where $\sin\beta = -(2N/\pi\omega_m^3 LC)(d\omega/dm)$ is obtained by differentiating $\cos\beta \simeq [1 + (M/L) - (1/\omega_m^2 LC)]$ with respect to m. Substituting into (B.5) and using (B.2) gives an approximation for the input impedance (23) in the neighborhood of the mth mode resonance:

$$\boldsymbol{Z}^{\text{eq}}_{\text{in}} \simeq \frac{\boldsymbol{Z}_1}{2}(N_f - N_g) + \frac{(1 - w_m^2 MC)D^2}{2N\boldsymbol{Y}_{\text{par}}}, \tag{B.6}$$

where $\boldsymbol{Y}_{\text{par}}$ is the admittance of a parallel resonance circuit having C in parallel with the series combination of L and R':

$$\boldsymbol{Y}_{\text{par}} \simeq \frac{1}{R'Q^2}\left[1 + j2Q\frac{d\omega}{\omega_m}\right], \tag{B.7}$$

and $Q = \omega_m L/R'$ is the quality factor of the antenna at the resonance frequency of the mth mode. Expressions (30)–(35) follow directly.

References

[1] Lieberman M A and Lichtenberg A J 2005 *Principles of Plasma Discharges and Materials Processing* 2nd edn (Hoboken, NJ: Wiley)
[2] Guittienne Ph, Lecoultre S, Fayet P, Larrieu J, Howling A A and Hollenstein Ch 2012 *J. Appl. Phys.* **111** 083305
[3] Lecoultre S, Guittienne Ph, Howling A A, Fayet P and Hollenstein Ch 2012 *J. Phys. D: Appl. Phys.* **45** 082001
[4] Guittienne Ph, Fayet P, Larrieu J, Howling A A and Hollenstein Ch 2012 *55th Annual SVC (Surface Vacuum Coaters) Technical Conf. (Santa Clara, CA, 28 April–3 May)*
[5] Jin J 1998 *Electromagnetic Analysis and Design in Magnetic Resonance Imaging* (Boca Raton, FL: CRC Press)
[6] Guittienne Ph, Chevalier E and Hollenstein Ch 2005 *J. Appl. Phys.* **98** 083304
[7] Hollenstein Ch, Guittienne Ph and Howling A A 2013 *Plasma Sources Sci. Technol.* **22** 055021
[8] Guittienne Ph 2010 Apparatus for large area plasma processing *Patent Specification* WO2010092433
[9] Novikov A 2011 *Magn. Reson. Imag.* **29** 260
[10] Pascone R J, Garcia B J, Fitzgerald T M, Vullo T, Zipagan R and Cahill P T 1991 *Magn. Reson. Imag.* **9** 395

[11] Tropp J 2002 *Concepts Magn. Reson.* **15** 177
[12] Hoult D I and Richards R E 1976 *J. Magn. Reson.* **24** 71
[13] Hayes C E, Edelstein W A, Schenck J F, Mueller O M and Eash M 1985 *J. Magn. Reson.* **63** 622
[14] Piejak R B, Godyak V A and Alexandrovich B M 1992 *Plasma Sources Sci. Technol.* **1** 179
[15] Kortshagen U, Gibson N D and Lawler J E 1996 *J. Phys. D: Appl. Phys.* **29** 1224
[16] Lieberman M A and Boswell R W 1998 *3rd Int. Workshop on Microwave Discharges J. Phys. IV France* **8** Pr7–145
[17] Cunge G, Crowley B, Vender D and Turner M M 1999 *Plasma Sources Sci. Technol.* **8** 576
[18] Zhao S-X, Xu X, Li X-C and Wang Y-N 2009 *J. Appl. Phys.* **105** 083306
[19] Gudmundsson J T and Lieberman M A 1998 *Plasma Sources Sci. Technol.* **7** 83
[20] Grover F W 1962 *Inductance Calculations: Working Formulas and Tables* (New York: Dover)
[21] Terman F E 1943 *Radio Engineer Handbook* (New York: McGraw-Hill)
[22] Wait J R 1961 *Proc. IRE* **49** 1576
[23] Bannister P R 1970 *Radio Sci.* **5** 1375
[24] Boteler D H and Pirjola R J 1998 *Geophys. J. Int.* **132** 31
[25] Keller J H, Forster J C and Barnes M S 1993 *J. Vac. Sci. Technol.* A **11** 2487